# Low-energy neutron direct capture by $^{12}$C in a dispersive optical potential

H. Kitazawa and K. Go
*Department of Energy Sciences, Interdisciplinary Graduate School of Science and Engineering, Tokyo Institute of Technology, 4259 Nagatsuta-cho, Midori-ku, Yokohama 226, Japan*

M. Igashira
*Research Laboratory for Nuclear Reactors, Tokyo Institute of Technology, 2-12-1 O-okayama, Meguro-ku, Tokyo 152, Japan*
(Received 12 June 1997)

A dispersive optical potential for the interaction between low-energy neutrons and $^{12}$C nuclei is derived from a dispersion relation based on the Feshbach generalized optical model. The potential reproduces completely neutron total cross sections below 1.0 MeV and substantially reproduces the energy of the 3090 keV($1/2^+$) level in $^{13}$C which is of nearly pure $2s_{1/2}$ single-particle character. It is found that direct-capture model calculations with this potential explain quite successfully the observed off-resonance capture transitions to the ground ($1/2^-$), 3090 keV($1/2^+$), 3685 keV($3/2^-$), and 3854 keV($5/2^+$) levels in $^{13}$C at neutron energies of 20–600 keV. Special emphasis is laid on the fact that in these model analyses, account should be taken of the spatial nonlocality of the neutron-nucleus interaction potential, in particular for negative energies. [S0556-2813(98)03201-4]

PACS number(s): 25.40.Lw, 24.10.Ht, 25.40.Hs, 27.20.+n

## I. INTRODUCTION

Low-energy neutron capture reactions on light nuclei play an important role in the nucleosynthesis on the inhomogeneous big-bang model as well as in the *s*-process nucleosynthesis in red giant stars. Recently, these findings have led to several measurements [1–4] of neutron capture cross sections of light nuclei at steller energies, which are compared to direct-capture model calculations [5] because the reactions can be decoupled from a resonance process.

Furthermore, drip-line light nuclei were found to have radii much larger than those of other neighboring nuclei [6]. This suggests the existence of a neutron-halo structure in the nuclei. A neutron halo is basically characterized by the presence of a weakly bound state which has an appreciable single-particle component of low angular momentum. The combination of the low neutron-separation energy and the low angular momentum allows neutrons to remain at distances much larger than the normal nuclear radius. Therefore, direct-capture model calculations [7,8] have been performed also with the expectation that the neutron-halo wave function could be probed by observing low-energy neutron direct-capture reactions on light nuclei.

Direct-capture transition amplitudes are generally quite sensitive to incoming wave functions in the nuclear channel region, i.e., to optical potential parameters used in the calculations. However, previous theoretical work [5,7,8] does not guarantee that the potential parameters reproduce the observed total cross sections and neutron single-particle bound state energies, and also does not make clear the relation of those parameters to available optical potentials obtained from neutron-scattering analyses.

In the present study, we intend to describe keV-neutron direct-capture reactions on $^{12}$C, using a dispersive optical potential which has a close connection with empirical optical potentials. Since no resonance has been observed in the $^{12}$C+$n$ interaction at neutron energies below about 2.0 MeV [9], this nucleus would be the most suitable for our theoretical analysis. The results are compared to recently observed off-resonance capture cross sections of $^{12}$C at 20–600 keV neutron energies [1–3].

## II. DISPERSIVE OPTICAL POTENTIAL

In this section, an optical potential for the interaction between low-energy neutrons and $^{12}$C nuclei is derived from a dispersion relation based on the Feshbach generalized optical model [10]. The real central part of this potential is described by the nonlocal Hartree-Fock and dispersive components. The Hartree-Fock component is approximated by an energy-dependent local potential whose strength decreases linearly with increasing neutron energy, while the dispersive component is represented by a dispersion relation that connects the real and imaginary parts of the optical potential. When the nonlocality of the imaginary (absorption) part of the single-particle field is neglected—in actuality the role of the nonlocality of the absorption potential is found to be small in theoretical investigations—the real central part $V(r,E)$ of the local dispersive optical potential is written as [11,12]

$$\begin{aligned} V(r,E) &= V_H(r,E) + \frac{P}{\pi}\int_{-\infty}^{\infty} \frac{W_S(r,E')}{E'-E}\,dE' \\ &= V_H(r,E) + \frac{2}{\pi}(E-E_F)P \\ &\quad \times \int_{E_F}^{\infty} \frac{W_S(r,E')}{(E'-E_F)^2-(E-E_F)^2}\,dE' \\ &= V_H(r,E) + \Delta V_S(r,E), \end{aligned} \tag{1}$$

where $P$ indicates a principal value. The potential $V_H(r,E)$ is the Hartree-Fock component, and $\Delta V_S(r,E)$ is the dispersive component due to the absorption potential $W_S(r,E)$,

 

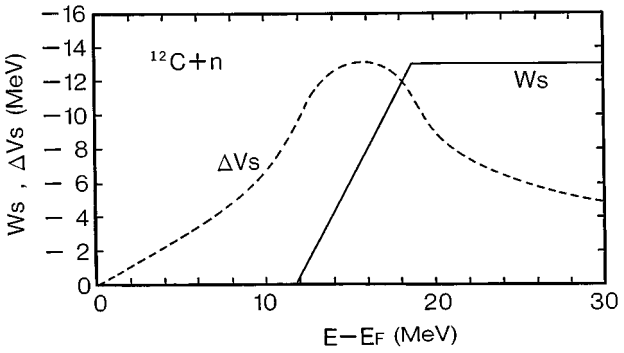


FIG. 1. Assumed surface absorption (solid line) and calculated dispersion (dashed line) potential depths for the $^{12}$C+$n$ interaction.

which is assumed to be symmetric about the Fermi energy $E_F$. Equation (1) shows how much of the energy dependence of empirical optical potentials arises from the nonlocality and how much from the dispersive nature of nuclear matter.

We determine a dispersive optical potential so as to be compatible with the Dave-Gould (DG) optical potential [13] from analyses of the elastic scattering of 7–15 MeV neutrons on $^{12}$C. The absorption potential is taken to be surface absorptive in the same way as the DG potential. It is well known that the volume absorption of an optical potential is not essential in MeV-neutron elastic scattering on $1p$-shell nuclei. In fact, the Watson-Singh-Segel (WSS) global optical potential of $1p$-shell nuclei [14] shows that the volume absorption is effective at neutron energies above 33 MeV.

The Hartree-Fock potential depth $V_H(E)$ is assumed to be the same as the real central part of the DG potential:

$$V_H(E) = -58.86 + 0.663E, \tag{2}$$

where $E$ is the center-of-mass energy in units of MeV. This potential acquires additional interest from the fact that the energy dependence of the real volume integral is consistent with that of the Jeukenne-Lejeune-Mahaux potential calculated from a realistic nucleon-nucleon interaction [13,15]. To be more exact, the Hartree-Fock potential should be obtained from an analysis of neutron elastic scattering on $^{12}$C using a dispersive optical potential, but since the dispersion potential due to surface absorption scarcely affects the neutron elastic scattering on $^{12}$C in the MeV-energy region, the above assumption for the Hartree-Fock potential is acceptable.

The absorption potential is required for the whole energy region before applying Eq. (1). In a scattering state, it is obtained from experiments with neutron elastic scattering on $^{12}$C. In a bound state, it can be deduced above the Fermi surface from the fragmentation of single-particle states observed by $^{12}$C$(d,p)$ reactions and below the Fermi surface from the fragmentation of single-hole states observed by $^{12}$C$(p,d)$ reactions. At present there is not enough information available to determine the energy dependence of the absorption potential strength at negative energies. However, near $E=0$ absorption potential strengths of global optical potentials of light nuclei are 1.0 MeV at most [14,16–18],

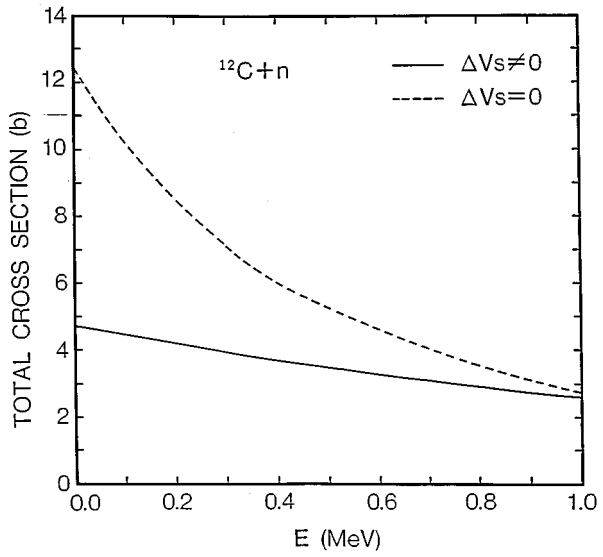


FIG. 2. Neutron total cross sections of $^{12}$C calculated using the dispersive optical potential with (solid line) and without (dashed line) the dispersion potential.

and therefore, at negative energies they would be a very small but nonzero value due to the coupling of a single-particle (or hole) state to other nuclear modes.

In the DG potential, the absorption potential depth increases linearly and very slowly with neutron energy: $W_S(E) = -12.65 - 0.045E$. No information is given on the dependence of the absorption potential upon neutron energies below 7 MeV. The imaginary component of the WSS potential decreases linearly with decreasing neutron energy below 13.8 MeV and becomes null at $E=0$. Above $E = 13.8$ MeV, the energy dependence is much weaker than that of the DG potential. From these facts, we assume an absorption potential depth shown by a solid line in Fig. 1: $W_S(E)=0$ at $E_F \leqslant E \leqslant 0$, $W_S(E) = -1.86E$ MeV at $0 \leqslant E \leqslant 7.0$ MeV, and $W_S(E) = -13.0$ MeV at $E \geqslant 7.0$ MeV. Using this absorption potential, the dispersion potential strength $\Delta V_S(E)$ is derived from the principal-value integral in Eq. (1), as shown by the dashed line in Fig. 1. The Fermi energy is defined as an average of the minimum energy $E_F^+$ of particle states and the maximum energy $E_F^-$ of hole states in $^{12}$C:

$$E_F = (E_F^+ + E_F^-)/2 = -11.83 \text{ MeV}. \tag{3}$$

Although the strength of the realistic absorption potential can be represented by a smooth function of neutron energy, a more complicated parametrization of the imaginary potential depth changes the dispersive correction only slightly.

The solid line in Fig. 2 shows the neutron total cross sections of $^{12}$C calculated using the dispersive optical potential. The potential form factors and spin-orbit potential depth are taken to be the same as those of the DG potential, except for the radius parameter $r_0$ of the Hartree-Fock potential. The dispersive optical potential $U_{\text{opt}}(r)$ used in the calculation is

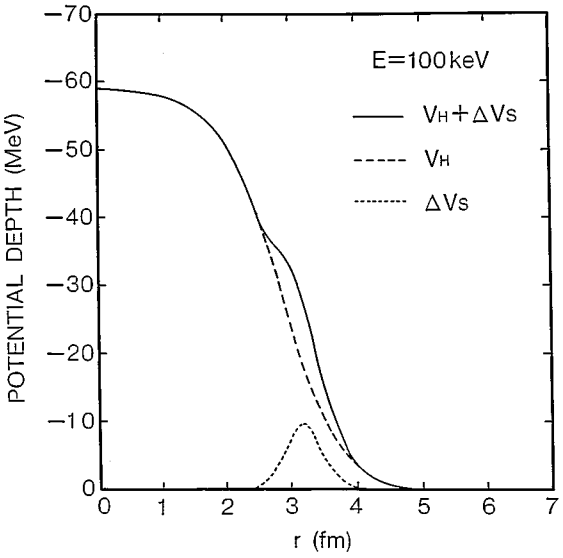


FIG. 3. Central part (solid line), Hartree-Fock component (dashed line), and dispersive component (dotted line) of the dispersive optical potential at the neutron energy of 100 keV.

$$U_{\rm opt}(r,E)=V_H(E)f(r,r_0,a_0)-4a_i\Delta V_s(E)\frac{df}{dr}(r,r_i,a_i)$$
$$-4ia_iW_s(E)\frac{df}{dr}(r,r_i,a_i)$$
$$-V_{\rm so}\lambda\!\!\!^{-2}_{\pi}(\boldsymbol{\sigma}\cdot\mathbf{l})\frac{1}{r}\frac{df}{dr}(r,r_{\rm so},a_{\rm so}), \qquad (4)$$

with

$$a_0=0.434\ \text{fm},\quad r_i=1.387\ \text{fm},\quad a_i=0.163\ \text{fm},$$
$$r_{\rm so}=1.15\ \text{fm},\quad a_{\rm so}=0.5\ \text{fm},\quad V_{\rm so}=-5.5\ \text{MeV},$$

where $\lambda\!\!\!^{-}_{\pi}$ is the pion Compton wavelength and $f$ is the Woods-Saxon form factor,

$$f(r,r_x,a_x)=[1+\exp\{(r-r_xA_{1/3})/a_x\}]^{-1}.$$

The radius parameter $r_0=1.211$ fm in the DG potential is slightly increased at lower neutron energies so as to completely reproduce the ENDF/B-V total cross sections [19]: $r_0=1.211$ fm at $E=1.0$ MeV to $r_0=1.229$ fm at $E=10$ keV. Such a small change of the radius parameter would not be unexpected since the optical potential describes only an average over partial waves, while the total cross sections at those neutron energies are dominated by very few partial waves. On the other hand, the optical potential with $\Delta V_S(E)=0$ overestimates the total cross sections, and the discrepancy between the calculated and ENDF/B-V values greatly increases with decreasing neutron energy. In other words, the dispersive correction is important for reproducing the total cross sections, especially at lower neutron energies.

A physical explanation of the characteristic behavior of the total cross sections is given in Figs. 3 and 4. As seen in Fig. 3, the addition of $\Delta V_S(r,E)$ is equivalent to increasing the radius parameter $r_0$ for the calculation which uses only a Woods-Saxon potential. Consequently, in the low-energy region where there is no essential contribution of partial waves with high angular momentum $l>0$, the incoming $s$ wave is pulled into the nuclear interior, and the total cross sections are decreased by the Ramsauer-like interference. For instance, the nuclear phase shift of the incoming $s$ wave at $E=100$ keV changes from 144° to 157° with the addition of the dispersive component (see Fig. 4).

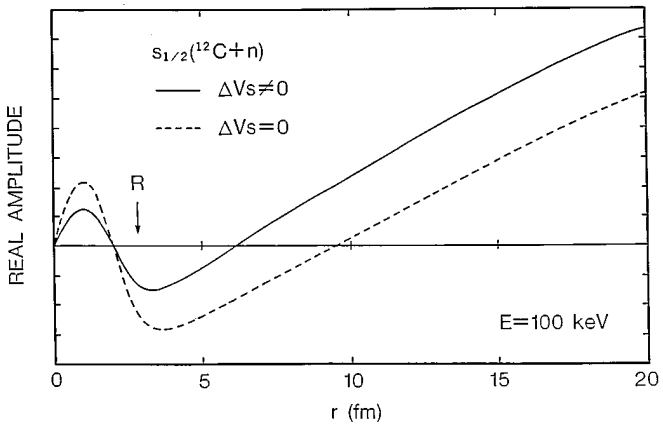


FIG. 4. Scattering $s$-wave functions calculated using the dispersive optical potential with (solid line) and without (dashed line) the dispersion potential at the neutron energy of 100 keV.

The observed total cross sections are also reproduced by the calculation which uses the optical potential without the dispersive component, but with a considerable increase of the radius parameter $r_0$ of the Hartree-Fock potential at lower neutron energies. However, such a strong energy dependence of the nuclear radius is unlikely to be a physical reality.

## III. MODEL CALCULATIONS AND DISCUSSION

The electric-dipole transition amplitude $T_{fi}$ for the radiative nucleon direct-capture process is

$$T_{fi}=\langle\Psi_f|\varepsilon|\Psi_i^{(+)}\rangle, \qquad (5)$$

where $\Psi_i^{(+)}$ is the initial elastic-scattering state wave function, whose incoming part is taken to be identical to that of the incident plane wave, $\Psi_f$ is the single-particle component of a final bound state, and $\varepsilon$ [$=\overline{erY_{1\mu}(\theta,\varphi)}$] is the electric-dipole operator for an incident nucleon. Using Eq. (5), we find the cross section for the neutron direct capture by an even-even nucleus:

$$\sigma_{fi}=\frac{8\pi}{3\hbar}k_\gamma^3\overline{e^2}\theta^2\sum_{j_il_i}G(l_ij_i,l_fj_f)|\langle r\rangle|^2, \qquad (6)$$

with

$$G(l_i,j_i,l_fj_f)=\frac{1}{2}(l_i+l_f+1)(2j_i+1)(2j_f+1)$$
$$\times\begin{Bmatrix}1 & l_i & l_f\\ 1/2 & j_f & j_i\end{Bmatrix}^2 \qquad (7)$$

and

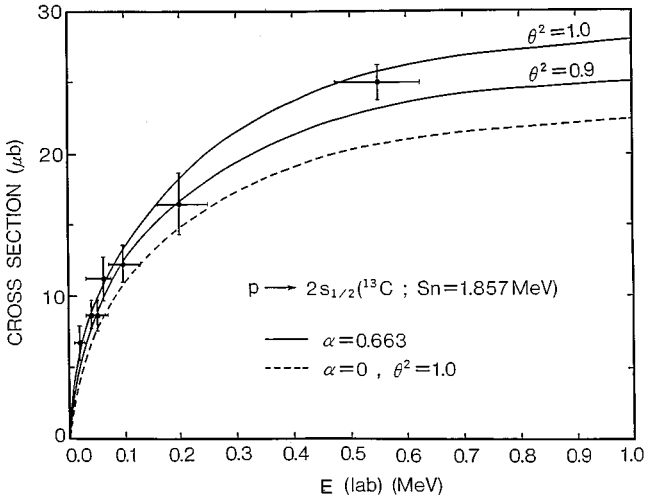


FIG. 5. Observed and calculated cross sections for the radiative neutron capture to the 3090 keV($1/2^+$) level in $^{13}$C. Solid ($\alpha \neq 0$) and dashed ($\alpha = 0$) lines represent calculations for the $p$-wave direct capture to the $2s_{1/2}$ single-particle state with a different spectroscopic factor.

$$\langle r \rangle = \int_0^\infty u_f(r) r u_i(r) dr, \tag{8}$$

where $k_\gamma$ is the wave number of capture gamma rays, $\overline{e}$ [$= -Ze/(A+1)$] is the neutron effective charge for the $E1$ transition in the potential produced by a target nucleus with mass number $A$ and atomic number $Z$, and $\theta^2$ is the spectroscopic factor of a final neutron single-particle state with principal quantum number $n_f$, orbital angular momentum $l_f$, and total spin $j_f$. The radial wave function $u_i(r)$ of an initial single-particle state has the asymptotic form

$$u_i(r) \sim -\frac{1}{2ikv^{1/2}} \left[ \exp\left\{ -i\left( kr - \frac{1}{2} l_i \pi \right) \right\} - S \exp\left\{ i\left( kr - \frac{1}{2} l_i \pi \right) \right\} \right], \tag{9}$$

where $k$ is the wave number of an incident neutron with velocity $v$ and $S$ is the scattering matrix element for the $(l_i j_i)$ partial wave. The wave function $u_i(r)$ is obtained as a solution of the Schrödinger equation with the dispersive optical potential in Eq. (4). The radial wave function $u_f(r)$ of a final single-particle state is determined by adjusting the depth of the Hartree-Fock term of this potential so as to reproduce the neutron binding energy $S_n$. Previous studies [5,7] assert that the wave functions of the initial and final single-particle states should be made orthogonal to each other, but we note that each nuclear state in general is described by a coupled-channel wave function so that there exists no orthogonality between both single-particle states.

In Fig. 5 the calculated capture cross sections for the transition to the 3090 keV($1/2^+$) level in $^{13}$C which has a large component of the $2s_{1/2}$ single-particle state are compared to recent measurements [1–3]. The dashed line shows calculations for the $p$-wave direct capture to the pure $2s_{1/2}$ single-particle state. The model calculations predict the cross sections to be about 20% smaller than those observed. An unphysical spectroscopic factor of 1.25 is then necessary to reproduce this experimental data. As shown below, this discrepancy can be removed by considering the spatial nonlocality of the microscopic mean field for the interaction between low-energy neutrons and $^{12}$C nuclei.

According to the work of Dover and Giai [20] and de Forest [21], the following relation exists between the wave functions $U_\lambda(r)$ and $u_\lambda(r)$ in equivalent nonlocal and energy-dependent local potentials:

$$U_\lambda(r) = P(r) u_\lambda(r), \tag{10}$$

with

$$P(r) = [m^*(r)/m]^{1/2}, \tag{11}$$

where $m^*(r)$ is the nucleon effective mass. The factor $[m^*(r)/m]^{1/2}$ which connects $U_\lambda(r)$ and $u_\lambda(r)$ leads, in the nuclear interior, to damping of the nonlocal wave function relative to the local one. This damping effect was first found by Perey [22], and is therefore referred to as the Perey damping factor. In the Hartree-Fock approximation, the effective mass $m_H^*(r)$ is equal to

$$m_H^*(r)/m = 1 - \frac{d}{dE} V_H(r,E). \tag{12}$$

Assuming a linear energy dependence of the Hartree-Fock potential depth, the Perey damping factor $P(r)$ is

$$P(r) = [1 - \alpha f(r)]^{1/2}. \tag{13}$$

In the present study, $\alpha$ is taken to be 0.663 from Eq. (2) and $f(r)$ is the Woods-Saxon form factor of the local Hartree-Fock potential. The single-particle bound state wave function $u_f(r)$ presented above in the local Hartree-Fock potential is then modified in the nonlocal potential as follows:

$$U_f(r) = C_f P(r) u_f(r), \tag{14}$$

where $C_f$ is introduced for normalizing $U_f(r)$. Equation (14) holds exactly for the Skyrme-Hartee-Fock approximation.

Introduction of the nonlocal interaction would also require modification of the electric-multipole moments. For a system of interacting nucleons, the expression for the charge-current density may differ from the corresponding expression for free nucleons. Thus the electromagnetic interaction $-(1/c)\int \mathbf{j} \cdot \mathbf{A}\, d\tau$ between the current density $\mathbf{j}$ and the vector potential $\mathbf{A}$ of a radiation field does not produce the well-known electric-multipole moments. However, in the limited case of nonrelativistic nucleon velocities and of radiation wavelengths large compared to the nuclear dimension, the nucleon interactions are expected to have a relatively minor effect on the electric-multipole moments [23,24], and therefore, in the present study the nonlocality of the nucleon potential is neglected for the electric-dipole interaction.

When $u_i(r)$ and $u_f(r)$ in Eq. (8) are replaced by $U_i(r)$ and $U_f(r)$, the calculations for the $p$-wave direct capture to the pure $2s_{1/2}$ single-particle state overestimate slightly the capture cross sections for the transition to the 3090 keV($1/2^+$) level, as shown by a solid line in Fig. 5. The best fit with the experimental data through adjusting the spectroscopic factor, gives $\theta^2 = 0.95$. This value has excel-

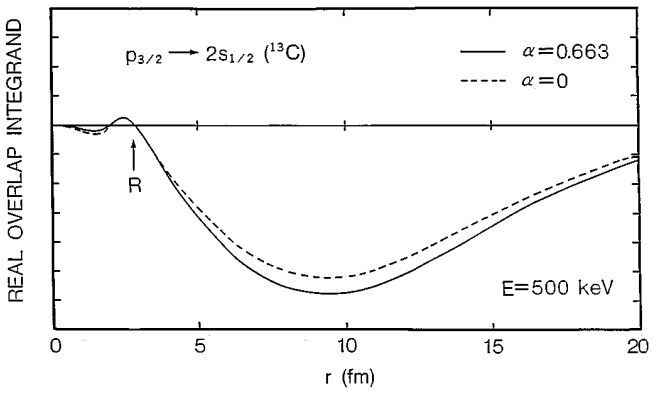


FIG. 6. Real overlap integrands of the transition amplitude for the $p_{3/2}$-wave direct capture to the $2s_{1/2}$ single-particle state at the neutron energy of 500 keV. Solid ($\alpha \neq 0$) and dashed ($\alpha = 0$) lines represent calculations using the dispersive optical potential.

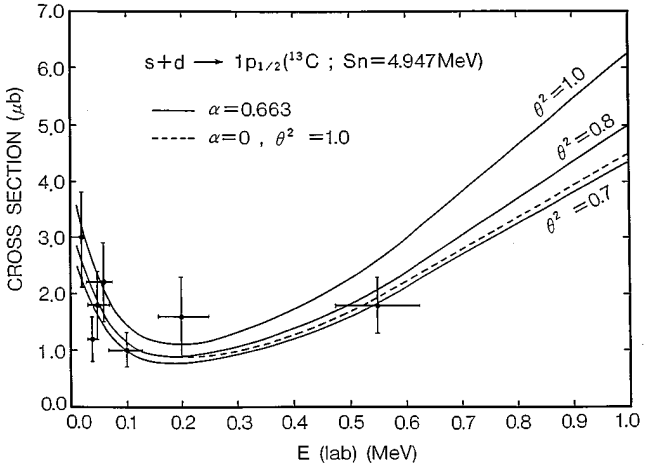


FIG. 7. Observed and calculated cross sections for the radiative neutron capture to the ground ($1/2^-$) level in $^{13}$C. Solid ($\alpha \neq 0$) and dashed ($\alpha = 0$) lines represent calculations for the $s$- and $d$-wave direct capture to the $1p_{1/2}$ single-particle state with a different spectroscopic factor.

lent agreement with the configuration-mixing ratio (94%) of the $(0 \otimes s_{1/2})$ component, which is theoretically predicted by taking account of the excitation of the $0_1^+$, $2_1^+$, and $4_1^+$ core ($^{12}$C) states in $^{13}$C [25]. Excluding the excitation of the $4_1^+$ core state, the core-particle model calculations produce a configuration-mixing ratio of 87% for the single-particle component [26], but the experimental data indicate participation of the $4_1^+$ state in the core excitation. From an experiment on the $^{12}$C$(d,p)$ $^{13}$C reaction, Takai *et al.* [27] also obtained evidence which indicated a nearly pure single-particle character of this level. The experiment by Ohnuma *et al.* [25] led to a rather small spectroscopic factor of 0.65. However, such a small value should be rejected, because the neutron binding energy of this level is in substantial agreement with the energy of the $2s_{1/2}$ single-particle state, as shown later.

Figure 6 shows the real overlap integrand of the transition amplitude for the dominant $p_{3/2}$-wave capture to the $2s_{1/2}$ single-particle state. When the nonlocality is considered ($\alpha \neq 0$), the amplitude of the initial-state wave function in the nuclear interior is attenuated by the Perey damping factor of Eq. (13). As can be seen from the figure, the contribution of the nuclear interior to the transition amplitude is very small, and therefore the effect of the nonlocality is negligible. Meanwhile the amplitude of the single-particle bound state wave function is emphasized in the nuclear exterior due to damping of the wave function in the nuclear interior. Consequently, the direct-capture transition amplitude, which has a dominant contribution of the nuclear exterior, increases to reproduce the observed cross sections.

The negative and positive parts of the overlap integrand in the nuclear interior are completely canceled out, which makes the direct-capture cross sections rather insensitive to the Hartree-Fock potential depth. The direct-capture transition would be decoupled by this cancellation from excitation of the giant-dipole resonance (GDR), the $p_{1/2}$-wave negative resonance [ground ($1/2^-$) level in $^{13}$C] and the $p_{3/2}$-wave negative resonance [3685 keV($3/2^-$) level in $^{13}$C,] because the transition amplitude in the nuclear interior is responsible for the coupling between the single-particle and resonance transitions [28,29]. Using the direct-semidirect capture model (DSD) with a complex coupling [30–32], in fact it can be confirmed that the effect of the GDR excitation is less than 0.3% and negligible. Again, the negative resonances would be decoupled more completely because the $p_{3/2}$-wave resonance has a small single-particle component ($\theta^2 = 0.2$) and the $p_{1/2}$-wave resonance is too far away in the energy space to make a significant contribution. In this context the strong energy dependence of the central part of the DG potential, which originates mostly from the nonlocality, seems to be valid.

The Hartree-Fock potential depth producing the $2s_{1/2}$ single-particle state at the energy of the 3090 keV($1/2^+$) level is 62.5 MeV, which is close to the potential depth of 60.1 MeV derived from Eq. (2) for negative energies. It is naturally expected from the strong single-particle character of this level. For $\Delta V_S(E) = 0$, the potential depth is 66.4 MeV. That is, the dispersion potential at negative energies is very effective in reproducing the observed neutron binding energy using the Hartree-Fock potential depth in Eq. (2). The dispersion potential also has an appreciable effect in increasing the direct-capture cross sections: by 2% for the transition to the $2s_{1/2}$ single-particle state and by 5–7 % for the transitions to the $1p_{1/2}$, $1p_{3/2}$, and $1d_{5/2}$ single-particle states.

In Fig. 7 the observed capture cross sections for the transition to the ground ($1/2^-$) level in $^{13}$C are compared to the direct-capture cross sections for the transition to the $1p_{1/2}$ single-particle state. Each solid line represents calculations with a different spectroscopic factor. The dashed line shows the direct-capture cross sections for the transition to the pure $1p_{1/2}$ single-particle state, neglecting the nonlocality. Below $E = 200$ keV, the $s$-wave capture to this state is dominant and decreases with increasing neutron energy. Above $E = 200$ keV, the capture cross section rapidly increases, when the $d$-wave capture becomes dominant with increasing neutron energy. The calculations with $\theta^2 = 0.8$ best fit the experimental data and the spectroscopic factor is in excellent agreement with the value of 0.77 obtained by Ohnuma *et al.* [25]. The shell-model calculation of Cohen and Kurath [33]

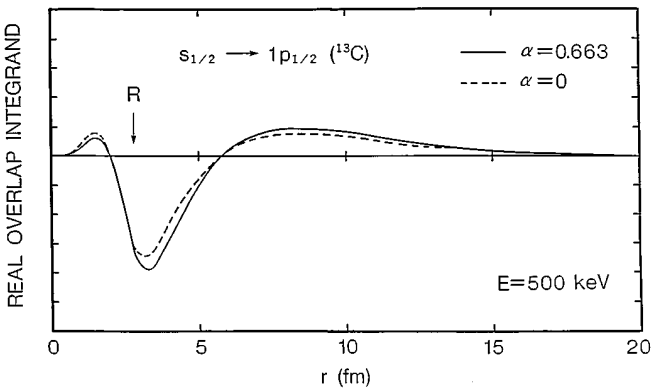


FIG. 8. Real overlap integrands of the transition amplitude for the $s$-wave direct capture to the $1p_{1/2}$ single-particle state at the neutron energy of 500 keV. Solid ($\alpha \neq 0$) and dashed ($\alpha=0$) lines represent calculations using the dispersive optical potential.

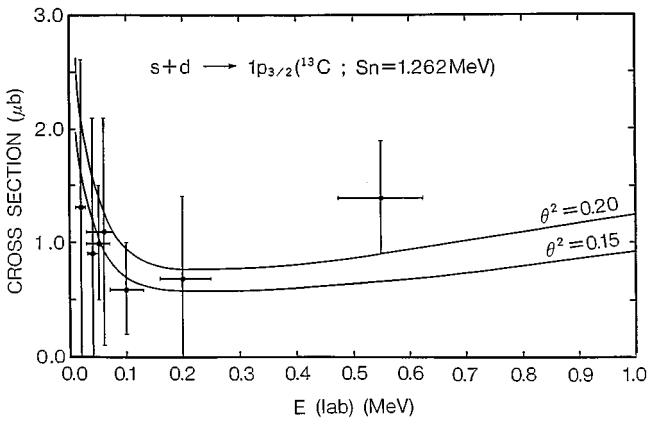


FIG. 9. Observed and calculated cross sections for the radiative neutron capture to the 3685 keV($3/2^-$) level in $^{13}$C. Solid lines represent calculations for the $s$- and $d$-wave capture to the $1p_{3/2}$ single-particle state with a different spectroscopic factor.

presents a rather small value of 0.61.

Figure 8 shows the real overlap integrand for the $s$-wave capture to the $1p_{1/2}$ single-particle state. There is no cancellation of the overlap integrand in the nuclear interior, and in addition the transition amplitude has this contribution of about 25% above $E=10$ keV. It is quite different from the $p \rightarrow 2s_{1/2}$ transition, and the direct-capture cross sections strongly depend on the Hartree-Fock potential depth used in the model calculation. Moreover, the large nuclear-interior contribution would give rise to the coupling of the direct-capture transition to the excitation of GDR and nearby resonances. When the GDR excitation is included, the DSD model calculations mentioned above show that the E1 transitions are considerably retarded: by 15–20 % below $E=100$ keV and by 6–7 % above $E=500$ keV. On the coupling to nearby resonances, the $s_{1/2}$-wave negative resonance [3090 keV($1/2^+$) level in $^{13}$C] with strong single-particle character would play a major role, because the resonance is located in the vicinity of the neutron-emission threshold [34]. However, it is not straightforward to make a quantitative estimation of the interplay of those resonance excitations coupled to the direct-capture transition, because there is still ambiguity in the model of the relative phases between all the processes concerned, the low-energy tail of the GDR profile, and the symmetry-potential form factor for light nuclei. In this respect, the deduced spectroscopic factor would include considerable uncertainty.

In Fig. 9 the observed capture cross sections for the transition to the 3685 keV($3/2^-$) level in $^{13}$C are compared to the direct-capture cross sections for the transition to the $1p_{3/2}$ single-particle state. This level is expected to have a small component of the $1p_{3/2}$ single-particle state, because the $1p_{3/2}$ shell in $^{13}$C is filled in the simple shell model. The calculations with a spectroscopic factor of 0.2 best fit the experimental data. The experiment of Takai *et al.* [27] produced $\theta^2=0.26$ and Ohnuma *et al.* [25] obtained a rather small value of 0.14. The shell-model calculation of Cohen and Kurath [33] predicts $\theta^2=0.19$. All of these spectroscopic factors are in substantial agreement with our value. The capture cross section gradually increases above $E=200$ keV with increasing neutron energy, because of the contribution of the $d$-wave capture. Figure 10 shows the real overlap integrand for the $s$-wave capture to the $1p_{3/2}$ single-particle state. Since the overlap integrand is not canceled out in the nuclear interior, but the contribution to the transition amplitude is only about 2% above $E=10$ keV, the direct-capture cross sections depend much more weakly on the Hartree-Fock potential depth, as compared to those for the $s_{1/2} \rightarrow 1p_{1/2}$ transition. The small contribution of the nuclear interior to the transition amplitude would also lead to a weakening the coupling between the direct-capture transition and the excitation of the $s_{1/2}$-wave negative resonance [3090 keV($1/2^+$) level in $^{13}$C] and $d_{5/2}$-wave negative resonance [3854 keV($5/2^+$) level in $^{13}$C] with a large single-particle component [34]. The effect of the GDR excitation is 3–4 %.

In Fig. 11 the direct-capture cross sections for the transition to the $1d_{5/2}$ single-particle state are compared to the observed capture cross sections for the transition to the 3854 keV($5/2^+$) level in $^{13}$C. Each solid line represents calculations for a different spectroscopic factor. The one that best fits the experimental data is made with $\theta^2=0.75$, which is in substantial agreement with the spectroscopic factor of 0.8 observed by Takai *et al.* [27]. The experiment of

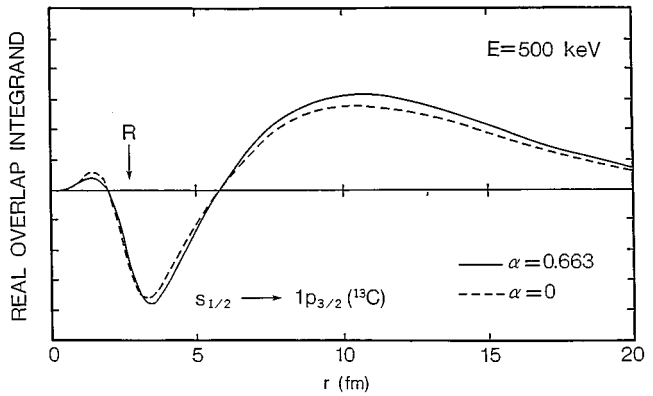


FIG. 10. Real overlap integrands of the transition amplitude for the $s$-wave direct capture to the $1p_{3/2}$ single-particle state at the neutron energy of 500 keV. Solid ($\alpha \neq 0$) and dashed ($\alpha=0$) lines represent calculations using the dispersive optical potential.

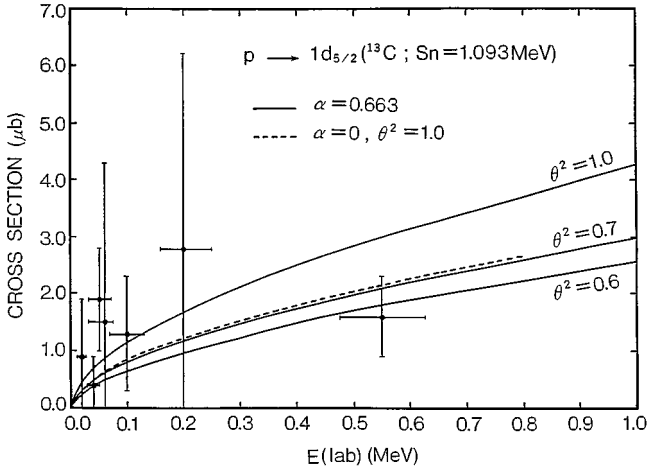


FIG. 11. Observed and calculated cross sections for the radiative neutron capture to the 3854 keV($5/2^+$) level in $^{13}$C. Solid ($\alpha \neq 0$) and dashed ($\alpha = 0$) lines represent calculations for the $p$-wave direct capture to the $1d_{5/2}$ single-particle state with a different spectroscopic factor.

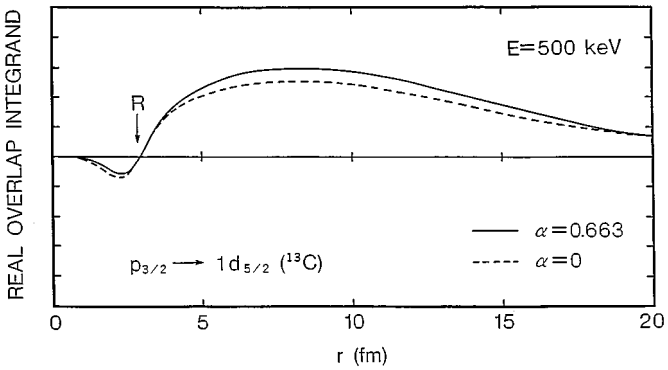


FIG. 12. Real overlap integrands of the transition amplitude for the $p_{3/2}$-wave direct capture to the $1d_{5/2}$ single-particle state at the neutron energy of 500 keV. Solid ($\alpha \neq 0$) and dashed ($\alpha = 0$) lines represent calculations using the dispersive optical potential.

Ohnuma *et al.* [25] produced a rather small value of 0.58. The core-particle model calculations mentioned above give a spectroscopic factor of 0.78, supporting our value. Figure 12 shows the real overlap integrand for the dominant $p_{3/2}$-wave capture to the $1d_{5/2}$ single-particle state. For this transition, the nuclear-interior contribution to the transition amplitude is very small, and therefore the direct-capture cross sections are rather insensitive to the Hartree-Fock potential depth. For a similar reason, the coupling between the direct-capture transition and the excitation of the GDR and $p_{3/2}$-wave negative resonance [3685 keV($3/2^-$) level in $^{13}$C] would be negligible.

As shown above, reasonable spectroscopic factors of the energy levels in $^{13}$C can be deduced from the neutron direct-capture model analysis considering the spatial nonlocality of the interaction potential. Disregarding the nonlocality, we find the larger spectroscopic factors: 1.0 for the ground ($1/2^-$) and 3854 keV($5/2^+$) levels (see Figs. 7 and 11) and 0.28 for the 3685 keV($3/2^-$) level, while the spectroscopic factor of the 3090 keV($1/2^+$) level greatly exceeds 1.0. In the meantime, when the $1p$ strength is exhausted by the $1/2^-$ and $3/2^-$ levels as the experiment of Ohnuma *et al.* [25] indicates, the sum-rule limit of those spectroscopic factors is 2.0. Without considering the nonlocality, the sum of the $(2J+1)\theta^2$ values for both levels is 3.1, which is much larger than the sum-rule limit.

As mentioned in Sec. II, the absorption potential in the present study includes some ambiguity at energies of $E_F$ to 7.0 MeV. As far as the radius parameter $r_0$ being adjusted to reproduce the total cross sections, reasonable variations (0–1.0 MeV) of the absorption potential strength at $E=0$ never affect the above results. When the absorption potential is drastically modified [$W_S(E) = -0.69E - 8.17$ MeV at $E_F \leqslant E \leqslant 7.0$ MeV and $W_S(E) = -13.0$ MeV at $E \geqslant 7.0$ MeV], the calculations below $E=500$ keV make a large overestimation of the capture cross sections for the transition to the ground ($1/2^-$) level. But the capture cross sections for the 3090 keV($1/2^+$) and 3854 keV($5/2^+$) transitions change only slightly (1–3 %). These facts are regarded as important results for validating the present analysis.

The direct-capture model calculations with the dispersive optical potential predicted by the WSS potential also have substantial agreement with the observed capture cross sections, using a spectroscopic factor of the nearly pure single-particle state for the ground ($1/2^-$) and 3090 keV($1/2^+$) levels. For this dispersive optical potential the effect of the nonlocality is somewhat indistinct due to the weak energy dependence ($\alpha = 0.3$) of the Hartree-Fock potential depth. As seen from the work of Dave and Gould, the energy dependence of the central part of the neutron optical potential is quite different for each light nucleus, indicating that nuclear individualities would be reflected in the nonlocality. The direct-capture model calculations should be performed with individual potential parameter sets, not with global ones.

## IV. SUMMARY

We determined the dispersive optical potential for the interaction between low-energy neutrons and $^{12}$C nuclei, which is compatible with the empirical optical potential obtained by Dave and Gould from neutron elastic scattering on $^{12}$C. The dispersive optical potential reproduces the ENDF/B-V neutron total cross sections below 1.0 MeV and, substantially, the energy of the 3090 keV($1/2^+$) level in $^{13}$C which is of strong single-particle character. The direct-capture model calculations with this potential are found to explain satisfactorily the observed capture transitions to four energy levels in $^{13}$C at neutron energies of 20–600 keV, considering the spatial nonlocality of the interaction potential for negative energies. The spectroscopic factors obtained from the model analyses are in reasonable agreement with those observed by the $^{12}$C$(d,p)^{13}$C reaction and/or theoretically calculated.

We would like to thank Prof. C. R. Gould of North Carolina State University and Triangle University Nuclear Laboratory for his valuable comments on neutron optical potentials of light nuclei.

[1] Y. Nagai, M. Igashira, K. Takeda, N. Mukai, S. Motoyama, F. Uesawa, H. Kitazawa, and T. Fukuda, Astrophys. J. **372**, 683 (1991).
[2] T. Ohsaki, Y. Nagai, M. Igashira, T. Shima, K. Takeda, S. Seino, and T. Irie, Astrophys. J. **422**, 912 (1994).
[3] Y. Nagai (private communication).
[4] M. Igashira, Y. Nagai, K. Masuda, T. Ohsaki, and H. Kitazawa, Astrophys. J. **441**, L89 (1995).
[5] A. Mengoni, T. Otsuka, and M. Ishihara, Phys. Rev. C **52**, R2334 (1995).
[6] I. Tanihata, H. Hamagaki, O. Hashimoto, Y. Shida, N. Yoshikawa, K. Sugimoto, O. Yamakawa, and T. Kobayashi, Phys. Rev. Lett. **55**, 2676 (1985).
[7] T. Otsuka, M. Ishihara, N. Fukunishi, T. Nakamura, and M. Yokoyama, Phys. Rev. C **49**, R2289 (1994).
[8] A. Mengoni, in Proceedings of the International Symposium on Neutron Capture Gamma-Ray Spectroscopy and Related Topics, Budapest, Hungary, 1996.
[9] S. F. Mughabghab, M. Divadeenam, and N. E. Holden, *Neutron Cross Sections* (Academic, New York, 1981), Vol. 1.
[10] H. Feshbach, Ann. Phys. (N.Y.) **5**, 357 (1958).
[11] C. Mahaux and H. Ngô, Nucl. Phys. **A378**, 205 (1982).
[12] C. Mahaux, H. Ngô, and G. R. Satchler, Nucl. Phys. **A449**, 354 (1986).
[13] J. H. Dave and C. R. Gould, Phys. Rev. C **28**, 2212 (1983).
[14] B. A. Watson, P. P. Singh, and R. E. Segel, Phys. Rev. **182**, 977 (1969).
[15] J.-P. Jeukenne, A. Lejeune, and C. Mahaux, Phys. Rev. C **16**, 80 (1977).
[16] S. G. Glendinning, S. El-Kadi, C. E. Nelson, R. S. Pedroni, F. O. Purser, and R. L. Walter, Nucl. Sci. Eng. **80**, 256 (1982).
[17] N. Olsson, B. Trostell, and E. Ramström, in *Proceedings of the International Conference on Nuclear Data for Science and Technology*, Mito, Japan, 1988, edited by S. Igarasi (Saikon, Tokyo, 1988), p. 1045.
[18] R. L. Walter, Triangle Universities Nuclear Laboratory Annual Report No. TUNL-XIX, 1980, p. 1.
[19] V. McLane, C. L. Dunford, and P. F. Rose, *Neutron Cross Sections* (Academic, New York, 1988), Vol. 2.
[20] C. B. Dover and N. V. Giai, Nucl. Phys. **A190**, 373 (1972).
[21] T. de Forest, Nucl. Phys. **A163**, 237 (1971).
[22] F. G. Perey, in *Proceedings of the Conference on Direct Interactions and Nuclear Reaction Mechanisms*, edited by E. Clementel and C. Villi (Gordon and Breach, New York, 1963), p. 125.
[23] A. J. F. Siegert, Phys. Rev. **52**, 787 (1937).
[24] A. Bohr and B. R. Mottelson, *Nuclear Structure* (Benjamin, New York, 1969), Vol. I, p. 379.
[25] H. Ohnuma, N. Hoshino, O. Mikoshiba, K. Raywood, A. Sakaguchi, G. G. Shute, B. M. Spicer, M. H. Tanaka, M. Tanifuji, T. Terasawa, and M. Yasue, Nucl. Phys. **A448**, 205 (1985).
[26] M. Tanifuji, O. Mikoshiba, and T. Terasawa, Nucl. Phys. **A388**, 621 (1982).
[27] M. Takai, T. Kambara, K. Tada, M. Nakamura, and S. Kobayashi, J. Phys. Soc. Jpn. **43**, 17 (1977).
[28] H. Kitazawa, M. Igashira, S. Shibata, K. Tanaka, H. Takakuwa, and K. Masuda, Nucl. Phys. **A575**, 72 (1994).
[29] H. Kitazawa, M. Igashira, M. Shimizu, K. Muto, T. Oda, Y. Achiha, Y.-H. Lee, and N. Mukai Phys. Rev. C **46**, 2364 (1992).
[30] M. Potokar, Phys. Lett. **46B**, 346 (1973).
[31] H. Kitazawa, Triangle Universities Nuclear Laboratory Annual Report No. TUNL-XIX, 1980, p. 114.
[32] H. Kitazawa, computer code HIKARI (unpublished).
[33] S. Cohen and D. Kurath, Nucl. Phys. **A101**, 1 (1967).
[34] Yu-Kun Ho, H. Kitazawa, and M. Igashira, Phys. Rev. C **44**, 1148 (1991).